polymer papers

X-ray structural study of oriented vinylidene fluoride/trifluoroethylene copolymers

J. A. Day, E. L. V. Lewis* and G. R. Davies
IRC in Polymer Science and Technology, Leeds University, Leeds LS2 9JT, UK
(Received 6 February 1991; accepted 24 April 1991)

The orientation of the crystalline regions in the vinylidene fluoride/trifluoroethylene (VDF/TrFE)-copolymer with molecular ratio 70:30 has been studied by wide-angle X-ray diffraction. This copolymer crystallizes in the β-phase or form I upon compression moulding. Dumb-bells 90 mm wide by 50 mm long were drawn at 0.25 mm min^{-1} and 80–85°C to the natural draw ratio of 7; the oriented sheets were void-free, and the crystal phase remained form I. Some samples were then poled at 200 MV m^{-1}. Strips 0.5 mm wide of both unpoled and poled samples were examined in a two-circle X-ray diffractometer, and all equatorial ω scans corrected for absorption of the X-ray beam. Both (200/110) and (310/020) composite reflections then showed six distinct intensity maxima round the draw direction, separated by 60° from each other, indicating a high degree of uniplanar–axial orientation within the drawn sheets. Calculation of the structure factors from two crystal models and comparison with the measured intensity ratios round the draw direction by curve-fitting methods showed that most of the polar *b* axes of the unpoled material are in the sheet plane (*bc* sheets), and that poling increases the number of these axes taking on positions 60° from this plane, in line with similar results in the poly(vinylidene fluoride) homopolymer.

(Keywords: vinylidene fluoride; trifluoroethylene; copolymers; X-ray diffraction; poling; uniplanar–axial orientation)

INTRODUCTION

The crystal structure adopted by a vinylidene fluoride/trifluoroethylene (VDF/TrFE) copolymer depends upon the composition, preparation technique and thermal history of the material. Copolymers with a VDF content of 60–80% spontaneously crystallize into a low-temperature crystal phase[1,2] similar to the β-phase or form I of PVDF[3]. Tashiro *et al.*[4,5] report that this low-temperature phase is monoclinic with $\beta = 93°$, although most workers assume an orthorhombic structure with dimensions rendering it 'pseudo-hexagonal'. The molecular chains are in the all-*trans* zigzag conformation and are packed in a parallel array, giving a highly polar phase.

In order to produce a macroscopically polar sample, the material must be poled in a high electric field. It has been shown through X-ray[6–9], electric displacement[10–14], and infrared[15–17] measurements that the strong polarization imparted to PVDF and its polar copolymers is mainly associated with ferroelectric dipole reorientation in the crystalline regions. Ferroelectric switching of the polarization in the crystals has been considered by a number of authors. Kepler and Anderson[8] have suggested a model related to the pseudo-hexagonal character of the form I crystals so that polarization occurs by rotations of the dipoles in 60° increments. A similar mechanism, proposed by Broadhurst *et al.*[18], argues for a six-site potential-well cooperative model; and calculated hysteresis curves mimic the experimental curves quite well. Much experimental evidence has since confirmed that the dipoles of form I PVDF and low-temperature P(VDF/TrFE) are oriented by 60° steps in the direction of the poling field[1,9,19–23].

In this paper, we investigate the structure of oriented VDF/TrFE copolymer samples in the molar ratio 70:30. It will be shown that the oriented samples, drawn from dumb-bells with a low length-to-width aspect ratio, are not cylindrically symmetric about the draw direction. We will also examine the polarization behaviour of the samples. Results are consistent with proposals that macroscopic polarization occurs by 60° step rotations of the crystalline dipoles into the direction of the poling field.

SAMPLE PREPARATION

P(VDF/TrFE) pellets, in the molar ratio 70:30, were manufactured by Atochem Ltd, France. Sheets of thickness 0.45 mm were produced by compression moulding the pellets at a temperature of 205°C in a hydraulic press. These sheets were quenched directly into water at room temperature. Dumb-bells with a gauge length of 50 mm and a width of 90 mm were cut from the sheets. Oriented samples were obtained by drawing these low-aspect-ratio dumb-bells at a draw rate of 0.25 mm min^{-1} and a temperature around 80–85°C. Samples produced were void-free, about 60 mm wide and 80 μm thick, and drawn to a natural draw ratio of 7 (OR7). The width, thickness and draw directions of the samples are defined as the 2, 3 and 1 directions respectively (*Figure 1*).

Vacuum-deposited aluminium electrodes were evaporated onto the surfaces of samples to be polarized. Polarization was achieved by applying a high d.c. voltage, corresponding to an electric field of 200 MV m^{-1}, across

* To whom correspondence should be addressed

0032-3861/92/081571-08

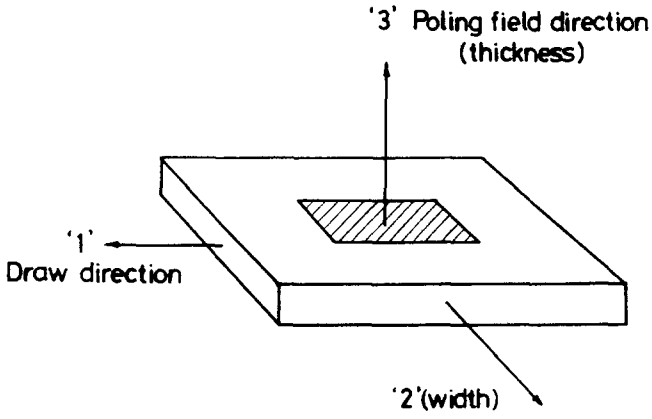

Figure 1 The axes notation

the electrodes at room temperature. During polarization, corona discharge and the associated electrical tracking was reduced by ensuring that the electrodes were not applied close to the edges of the samples and by immersing the samples in transformer oil.

Strip specimens, with typical lengths and widths of 30 mm and 0.5 mm respectively, were cut parallel to the 1 and 2 directions of the unpoled and poled drawn samples.

EXPERIMENTAL

A Siemens K-4 X-ray generator equipped with a type F diffractometer with omega drive was used to obtain diffraction scans in Ni-filtered Cu Kα radiation. Each strip specimen was mounted vertically on a goniometer head at the centre of the diffractometer table. Collimator slits used were chosen to ensure that the whole cross-sectional area of the specimen was always within the line-focused X-ray beam.

Equatorial and meridional 2θ scans were obtained from strip specimens cut parallel and perpendicular to the draw direction. Scans were obtained in reflection and transmission modes as shown in *Figure 2*.

The ω scans were obtained by rotating the specimen at an angular velocity $\dot{\theta}$ at constant 2θ. The intensity was recorded as a function of ω, where ω is defined as in *Figure 2*. These scans were obtained only from specimens cut parallel to the draw direction. Diffraction peaks that were observed then correspond to reflections from $(hk0)$ planes.

RESULTS AND DISCUSSION

The 2θ scans

In all the 2θ scans obtained, no crystal phase other than the low-temperature phase was present and, therefore, all discussion is made with respect to this phase. The diffraction peak positions of the scans obtained for the unpoled and poled specimens, whether taken in reflection or transmission modes, are not significantly different. Differential absorption effects prevented direct comparison of the peak intensities of the scans.

A typical equatorial scan is shown in *Figure 3*. The pseudo-hexagonal symmetry of the low-temperature phase results in many composite diffraction peaks. The peak positioned at $2\theta = 19.80°$ corresponds to reflections from the (200) and (110) planes. The broad shoulder on the low-angle side of this peak ($2\theta \sim 18.3°$) is due to diffraction from the amorphous regions of the material. The peak at $2\theta = 35.25°$ corresponds to reflections from the (310) and (020) planes. That at $2\theta = 40.85°$ corresponds to reflections from the (400) and (220) planes.

A typical meridional scan, performed in transmission mode only, is shown in *Figure 4*. The intense peak at

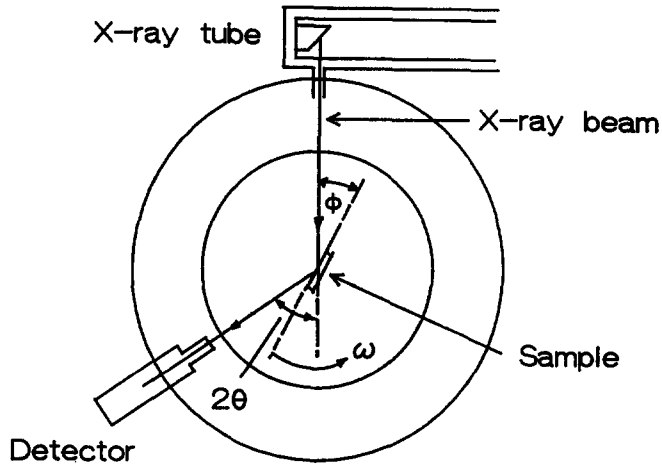

Figure 2 Plan of the X-ray diffractometer, showing the definition of the angles 2θ, ϕ and ω. The sample as shown is for the 2θ scan in the reflection-symmetrical mode, where $\phi = \theta$; for the transmission-symmetrical mode, $\phi = 90° + \theta$. For ω scans, 2θ is constant, and ω varied

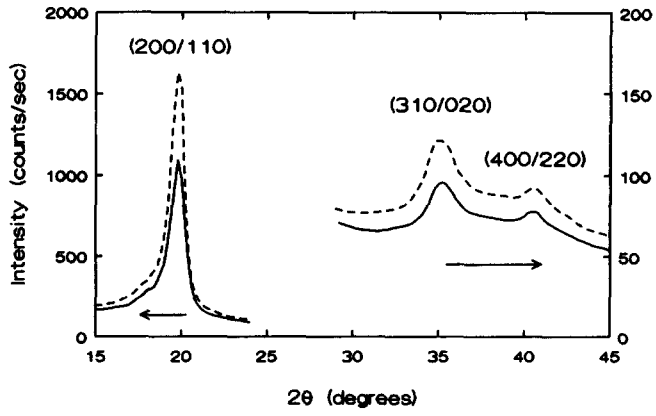

Figure 3 An equatorial scan of the poled copolymer; the unpoled sample is similar. The reflection and transmission modes are shown by the full and broken curves respectively

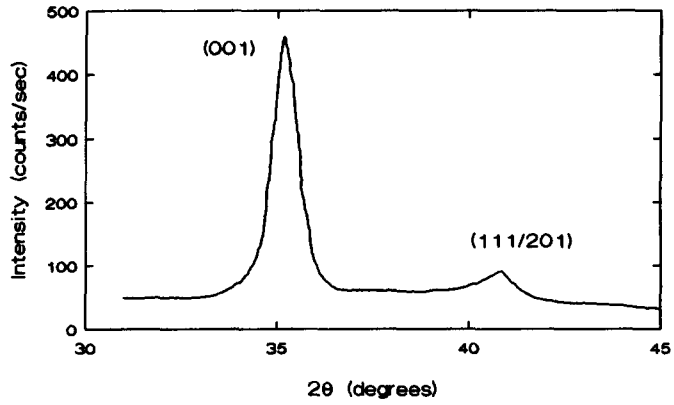

Figure 4 A meridional scan of the poled copolymer in the transmission mode. The unpoled sample is similar

$2\theta = 35.30°$ corresponds to reflections from the (001) planes. The low-intensity peak at $2\theta = 40.80°$ corresponds to reflections from the (111) and (201) planes because the orientation of the crystallographic axis is not perfect along the draw direction. There was no difference between the f.w.h.m. values (i.e. the widths of the peaks at half the maximum intensity above the background level) of the reflections observed for the unpoled and poled specimens. This observation, together with the fact that the peak positions of the reflections did not change on poling, leads to the conclusion that poling does not improve the packing of the crystalline chain segments or increase the perfection of the crystalline regions.

The ω scans

In a single low-temperature crystal, the crystalline planes of the (110/200) and of the (310/020) composite reflections are inclined at approximately 60° to each other (*Figure 5*). In a uniaxially drawn sample, the *c* axes of the crystallites are preferentially oriented along the draw direction and, therefore, the *a* and *b* axes lie in the plane perpendicular to the draw direction. The ω scan study was undertaken to determine the orientation of the crystallites around the draw direction in the unpoled and poled samples.

The ω scans were performed for the (200/110) and the (310/020) composite reflections in turn. The linear absorption coefficient of the low-temperature phase copolymer, in the molar ratio 70:30, irradiated with Cu Kα radiation was calculated as $2.18\ mm^{-1}$, as described by Buerger[24]. Consequently, differential absorption effects due to the cross-sectional area of the specimens cannot be ignored. For a given fixed 2θ, algorithms defining every possible path length of the incident and diffracted beam within the specimen were calculated as a function of ω. Therefore, the transmission of the X-ray beam through the specimen could be evaluated for any 2θ. The ω scans were corrected by dividing the experimental intensity by the transmission at each value of ω.

The uncorrected and corrected (200/110) ω scans of the unpoled and poled specimens are shown in *Figures 6* and *7*. In these and all other plots ω covers the range at least −20° to +400°. Here, $\omega = 0°$, 180° and 360° correspond to the reflection symmetrical (RS) position and $\omega = 90°$ and 270° correspond to the transmission symmetrical (TS) position. The effect of absorption is clearly visible on these plots, especially around the RS positions. The corrected scans clearly show six distinct intensity maxima, centred on the RS positions and at 60° intervals between them. The fact that the maxima are separated by 60° reflects the pseudo-hexagonal symmetry of the low-temperature phase, suggesting that uniplanar–axial orientation is present around the draw direction of the sheets.

The uncorrected and corrected (310/020) ω scans of the unpoled and poled specimens, shown in *Figures 8* and *9*, also display six intensity maxima, now centred on the TS positions and at approximately 60° between them.

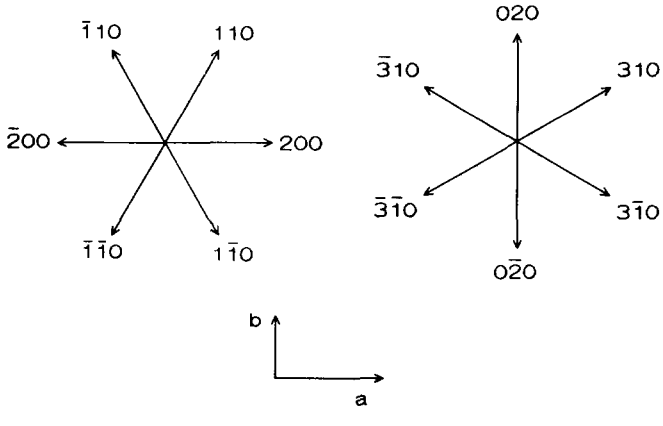

Figure 5 The directions of the plane normals in the crystal or a perfectly oriented sample, as seen down the *c* axis

Quantitative analysis of ω scans

In order to analyse the ω scans quantitatively, the structure factors of the low-temperature phase were required. The unit cell of this phase contains two monomer units from two molecular chains. There is a 70% probability that each monomer unit is a VDF segment and a 30% probability that it is a TrFE segment. The orthorhombic unit-cell dimensions were taken to be $a = 8.87$ Å, $b = 5.17$ Å and $c = 2.55$ Å. Bond lengths and angles were adopted from the work by Hasegawa[3] and Tashiro[4].

Two crystal models were proposed. The first model considers the molecular chains to be packed in planar zigzag form with each chain in the unit cell containing two carbon atoms C1 and C2, as shown in *Figure 10a*. C1 has one hydrogen atom H1b on one bond and either one fluorine atom F1a or one hydrogen atom H1a on the other. Carbon atom C2 has two fluorine atoms F2a and F2b bonded to it. The occupancy values assigned to atoms H1a and F1a are 0.35 and 0.15 respectively. All other atoms are assigned an occupancy of 0.5. Mirror planes normal to the *a* axis at $x = 0$ and $x = a/2$ ensure that atoms H1b and H1a or F1a are distributed either side of the chain, and also ensures that the total occupancy of each atom is unity.

The second model, shown in *Figure 10b*, is identical to model 1, except that now the CF_2 and CFH/CH_2 groups are statistically deflected from the planar zigzag conformation. The chains are deflected alternately to reduce the steric hindrance between the neighbouring non-bonded fluorine atoms. The model follows the work of Tashiro *et al.*[4] in proposing that internal rotations of the skeletal carbon–carbon linkages cause the CF_2 and CFH/CH_2 groups to be deflected from the *xy* plane. Atomic coordinates were deduced by interpolation of those of the statistically disordered model of Tashiro *et al.*, which describes the copolymer with a 55% VDF content, and the planar zigzag model of Hasegawa *et al.*[3], describing form I PVDF. In both models, an isotropic temperature factor $B = 5$ Å^2 was assumed for all atoms. The structure factors $F(hkl)$ and intensities $I(hkl)$ of the major reflections are presented in *Table 1*.

With reference to the work by Bur *et al.* on form I PVDF[9], it is proposed that the unpoled drawn copolymer samples are *bc* sheets. In this case, the dipoles lying parallel to the *b* axis of the low-temperature crystallites are preferentially oriented along the width direction of the sheet. Poling is thought to rotate the chains within the crystallites so that the dipoles end up as near as possible parallel to the poling field. The crystal structure constrains the dipoles so that rotations can take place only in 60° increments and, therefore, the dipoles tend to

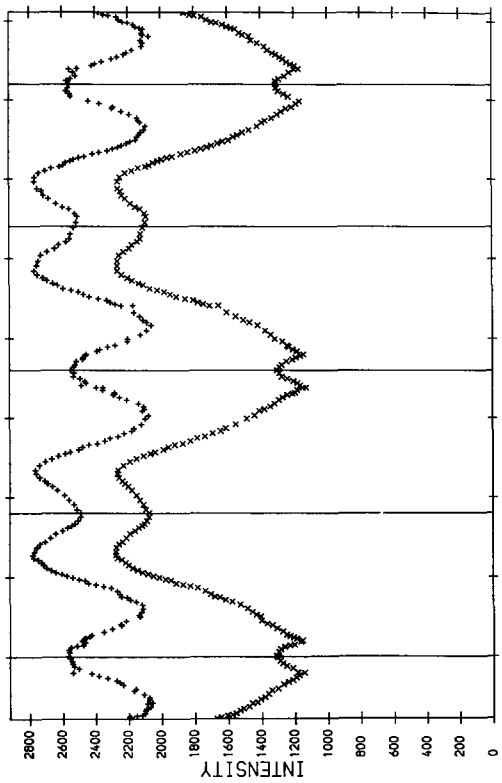

Figure 7 The (200/110) ω scans of the poled sample, uncorrected (×) and corrected for absorption (+)

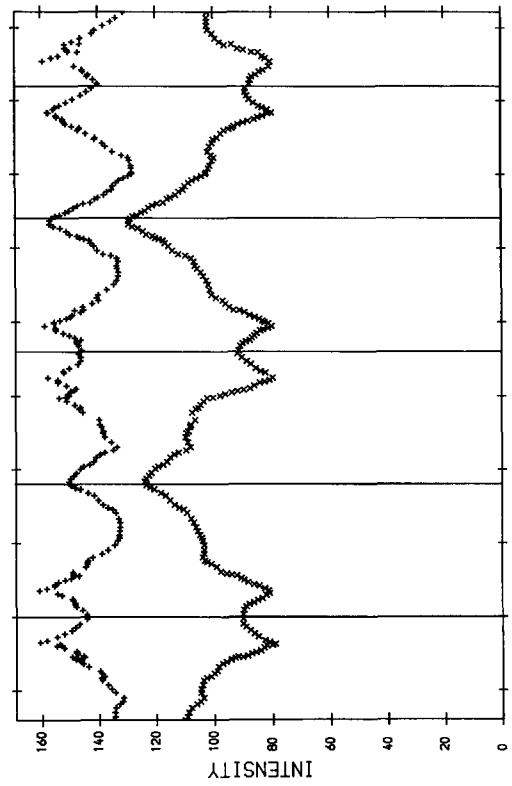

Figure 9 The (310/020) ω scans of the poled sample, uncorrected (×) and corrected for absorption (+)

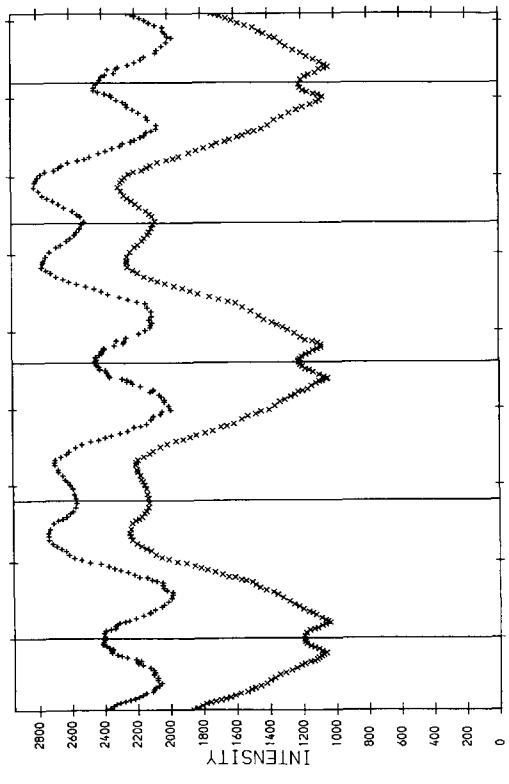

Figure 6 The (200/110) ω scans of the unpoled sample, uncorrected (×) and corrected for absorption (+)

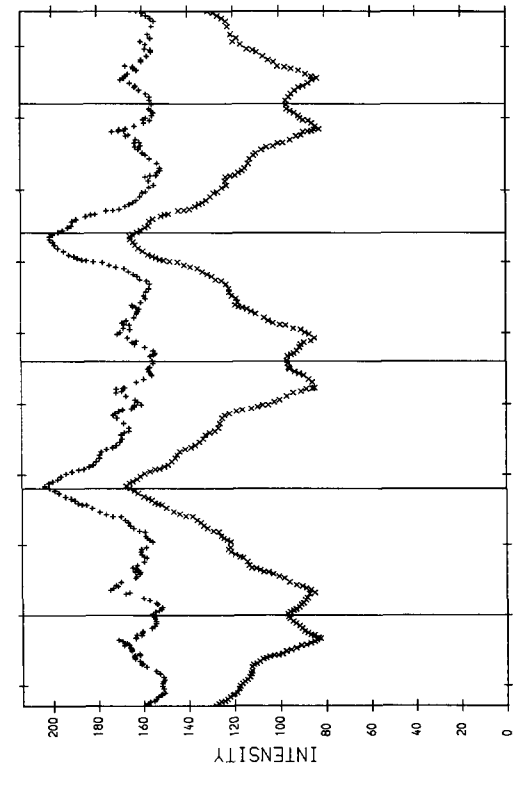

Figure 8 The (310/020) ω scans of the unpoled sample, uncorrected (×) and corrected for absorption (+)

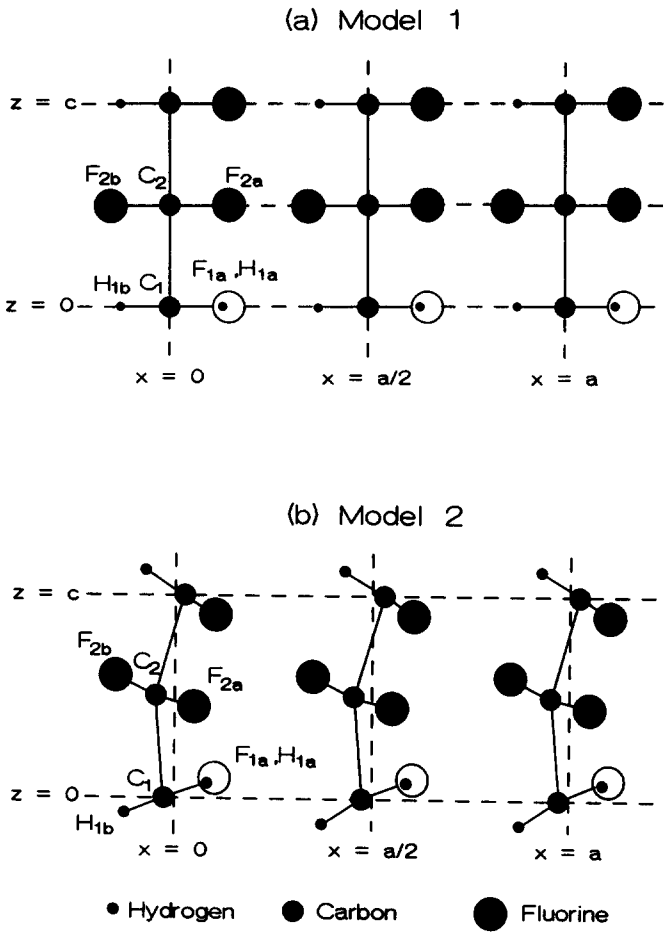

Figure 10 Crystal models for the 70/30 VDF/TrFE copolymer, as seen down the y axis: (a) planar zigzag chains; (b) with statistical deflections in the chains

Table 1 Structure factors and intensities of reflections calculated from the two models of the low-temperature phase

Reflection (hkl)	Model 1: planar zigzag		Model 2: statistically disordered	
	$\|F(hkl)\|$	$I(hkl)$	$\|F(hkl)\|$	$I(hkl)$
(200)	20.31	412.5	19.94	397.6
(110)	25.34	642.1	25.15	632.5
(310)	14.88	221.4	10.14	102.8
(020)	20.79	432.2	17.92	321.1
(400)	13.27	176.1	7.76	60.2
(220)	4.01	16.1	4.58	21.0
(001)	17.63	310.8	17.41	303.1
(111)	21.75	473.1	21.50	462.3
(201)	0.31	0.1	1.68	2.8

take up one of two positions at $\pm 30°$ to the poling direction. The effect is that the new crystal structure behaves like a twinned structure overall, with the new a and b axes at 30° and 60° respectively to the 2 direction in the 23 plane, the c axis remaining parallel to the draw direction.

A computer program was written to fit Gaussian functions in known positions of the ω scans. The program fits three parameters to the corrected ω scans: the height of each peak and the width of the peaks (f.w.h.m.). The latter should be the same for all equatorial reflections, if the degree of orientation of the c axes of the crystallites along the draw direction is much greater than that of the equatorial reflections in the plane normal to the draw direction. The positions of the peaks relative to each other are fixed by the symmetry of the crystallites. For example, if the (200) reflection is at $\omega = 0°$ (i.e. the RS position), then the (110) reflection will be at $\omega = \tan^{-1}(a/b) \sim 60°$. The background radiation of each corrected ω scan was found by measuring the background level beneath the corresponding equatorial 2θ scans, taken in reflection and transmission modes. These background levels, corrected for absorption, correspond to the background at the RS and TS positions of the ω scans. The variation of background with ω was taken to be sinusoidal, although the exact shape is not important because its variation from 0° to 90° is small. In all cases, the background radiation was accounted for in the curve-fitting routines.

The curve-fitting programe was used to fit the Gaussian peak shapes to the corrected (200/110) and (310/020) ω scans. The fitted ω scans are shown in *Figures 11–14*. The intensity ratios of the fitted peaks are defined as $I(60°)/I(0°)$ for the (200/110) scans and $I(90°)/I(30°)$ for the (310/020) scans. For each ω scan, the intensity ratio and widths of the fitted peaks are listed in *Table 2*. Theoretical intensity ratios were also calculated from the structure factors listed in *Table 1*, on the basis that the unpoled drawn samples are *bc* sheets and the poled drawn samples are completely poled with all the b axes of the crystallites oriented at $\pm 30°$ to the thickness direction.

The ratio of the fitted peak intensities of the (200/110) scans decreases from 1.28 to 1.17 on poling. Both of these ratios lie between the intensity ratios calculated from the theoretical models. This suggests that the unpoled samples are not pure *bc* sheets, and also that the poling process does not cause all the b axes to rotate by 60° increments towards the poling direction. The intensity ratios of the fitted (310/020) scans also lie between the theoretical ratios and decrease on poling. In all the scans, the widths of the fitted peaks before and after poling are not significantly different. This supports the view that dipoles rotate through discrete increments.

In order to investigate the degree of poling in the poled samples, it is necessary to deduce the distribution of b axes orientations about the draw direction. Consider the simple case in which the b axes are oriented along six directions fixed 60° apart as shown in *Figure 15*. If the total fraction of b axes that are oriented at $\pm 30°$ to the 3 direction is defined as f, then the fraction of b axes oriented parallel to the 2 direction is $(1 - f)$. The X-ray scans cannot be distinguish between dipoles oriented 180° apart and, therefore, the fraction f is equal to the total fraction of dipoles pointing at $\pm 30°$ and at $\pm 150°$ to the poling direction.

Table 2 Results of curve fitting to ω scans of OR7 sheets

	(200/110)		(310/020)	
	Unpoled	Poled	Unpoled	Poled
Intensity ratios				
Model 1	1.56	0.82	1.95	0.68
Model 2	1.59	0.81	3.12	0.49
Experimental	1.28	1.17	1.22	0.83
Peak width (deg)	54.2	53.4	53.6	56.2

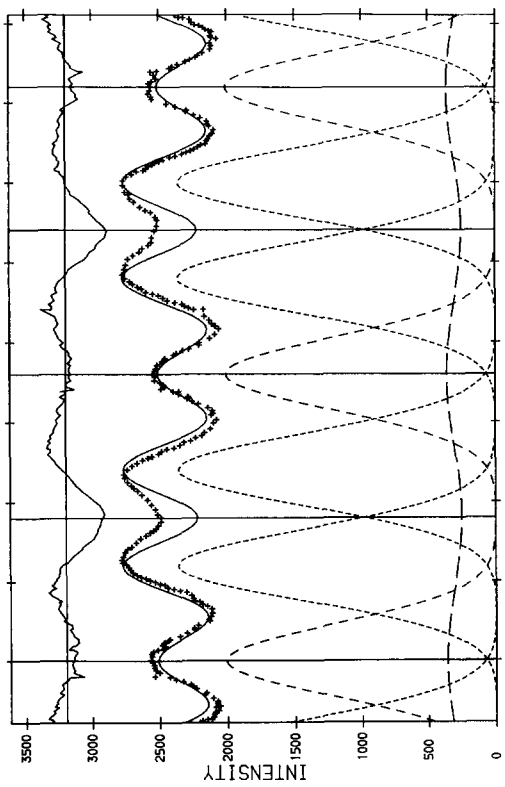

Figure 12 Corrected ω scans for the (200/110) reflections of the poled sample, with Gaussian peaks fitted. Notation as in *Figure 11*

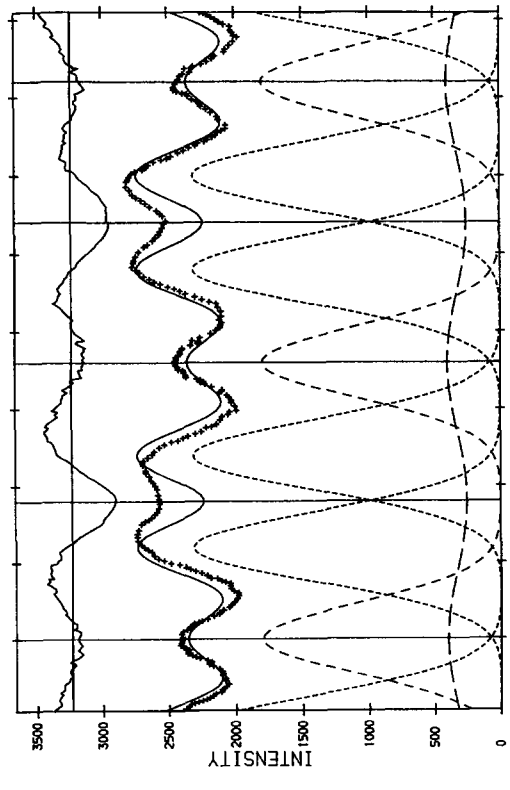

Figure 11 Corrected ω scans for the (200/110) reflections of the unpoled sample, with Gaussian peaks fitted: long dashes represent 200 reflections, short dashes 110 reflections and longest dashes the background; (+) represents the corrected scan, and the full curve around it is the best-fitted line. Above is the difference between the two

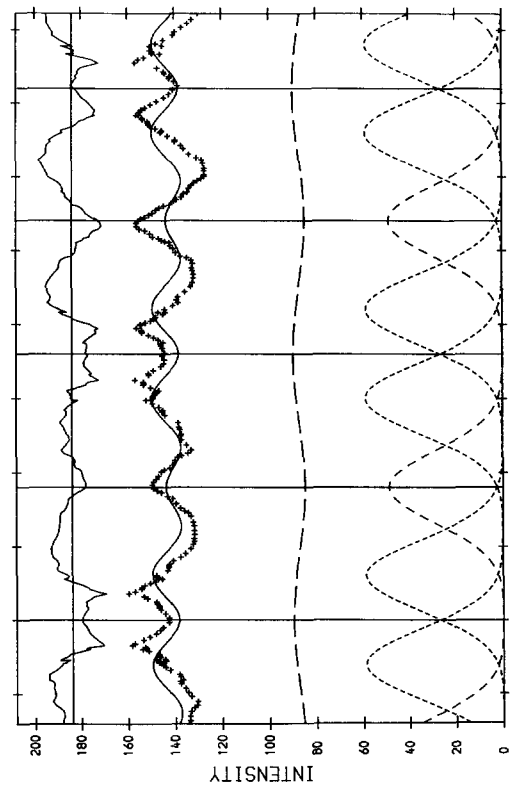

Figure 14 Corrected ω scans for the (310/020) reflections of the poled sample, with Gaussian peaks fitted. Notation as in *Figure 11*

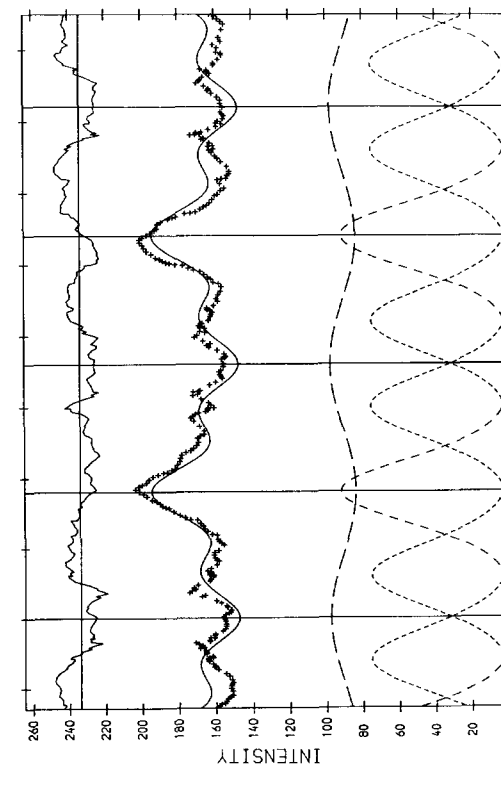

Figure 13 Corrected ω scans for the (310/020) reflections of the unpoled sample, with Gaussian peaks fitted. Notation as in *Figure 11*

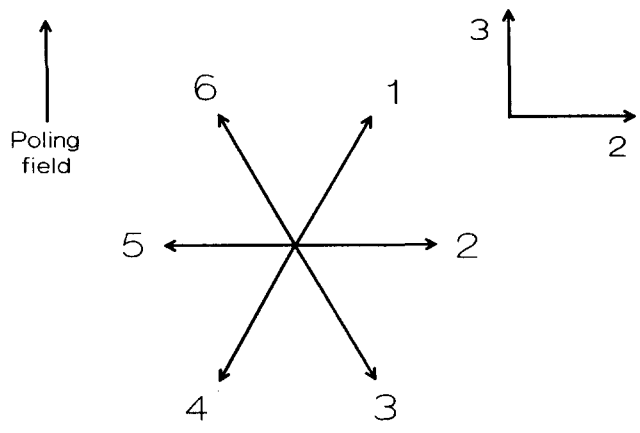

Figure 15 The six directions the *b* axes can adopt

Table 3 The fraction of *b* axes oriented at ±30° to the thickness direction in the OR7 sheets

	Model 1: planar zigzag		Model 2: statistically disordered	
ω scan	Unpoled (f_u)	Poled (f_p)	Unpoled (f_u)	Poled (f_p)
(200/110)	0.27	0.41	0.29	0.42
(310/020)	0.50	0.83	0.56	0.76

Now, considering the (200/110) ω scan, the fraction of (200) planes oriented at +60° or at −60° to the 3 direction is (f/2), and the fraction of (110) planes oriented at +60° or at −60° to the 3 direction is (1 − f/2). Also, the fraction of (200) planes oriented at 0° to the 3 direction is (1 − f), and the fraction of (110) planes oriented at 0° to the 3 direction is f. Therefore, the intensity ratio of the peaks positioned at ω = 60° to ω = 0° can be written as:

$$\frac{I(60°)}{I(0°)} = \frac{(2-f)I(110) + fI(200)}{2(1-f)I(200) + 2fI(110)} \quad (1)$$

where I(200) and I(110) are the intensities of the (200) and (110) reflections respectively.

In the same way, considering the (310/020) ω scan, it can be shown that the intensity ratio of the peaks at ω = 90° to ω = 30° is:

$$\frac{I(90°)}{I(30°)} = \frac{2(1-f)I(020) + 2fI(310)}{(2-f)I(310) + fI(020)} \quad (2)$$

where I(310) and I(020) are the intensities of the (310) and (020) reflections. Using the theoretical intensities of the reflections listed in *Table 1*, it can be seen that the cases f = 0 and 1 correspond to the pure *bc* sheet and the fully poled cases respectively.

Equations (1) and (2) have been used to calculate f from the experimental results using the intensity ratios of the fitted peaks and the theoretical intensities of the reflections. *Table 3* presents a summary of the results for the two theoretical models, where f_u and f_p are the unpoled and poled fractions respectively.

The values of f obtained for the (200/110) and (310/020) scans do not agree, either in the unpoled or poled cases. This discrepancy may be partly due to the uncertainty in the results of the (310/020) ω scans, owing to the low intensity of the reflections above the background radiation level. The above treatment does, however, highlight the increase in the fraction of *b* axes oriented at 30° to the 3 direction of the poled samples, thus supporting dipole orientation in 60° increments as the mode of polarization.

The mean orientation of the dipoles, θ_0, in the crystalline phase with respect to the poling direction depends upon the distribution of the dipoles in the 23 plane. Let us assume that the dipoles, oriented parallel with the *b* axes, occupy one of six fixed sites about the draw direction, as shown in *Figure 15*. If it is assumed that all the dipoles pointing at 30° to the 3 direction occupy sites 1 and 6, then the (200/110) scans give the fraction of dipoles pointing at 30° to the poling field as 0.42 and the fraction of dipoles pointing at 90° to the poling field as 0.58. This sets a maximum value on $\langle \cos \theta_0 \rangle = 0.36$, where the angular brackets imply the average over all the dipoles.

The above simple treatment neglects the fact that a small fraction of the dipoles may be oriented at ±150° to the poling field (i.e. sites 3 and 4). It also neglects the distribution of dipole orientations about each of the six fixed directions (i.e. that f.w.h.m. = 54°). These complications will tend to decrease the value of $\langle \cos \theta_0 \rangle$ still further. This low value arises because the *b* axes of most of the crystallites in the unpoled samples are preferentially oriented along the 2 direction. Although poling causes many of the dipoles to reorient at 30° to the field, the majority still remain along the 2 direction of the samples.

CONCLUSIONS

The wide-angle X-ray diffractometry study has given direct evidence supporting the six-site model of dipolar orientation in the low-temperature phase of P(VDF/TrFE). The presence of six intensity maxima in the equatorial ω scans is a consequence of the drawing process. The low length-to-width aspect ratio of the dumb-bells restricts contraction in the width direction of the material on drawing. This results in the oriented samples possessing uniplanar–axial orientation about the draw direction. The unpoled samples are *bc* sheets. Poling causes the polar *b* axes of the crystallites to rotate by 60° increments about the *c* axes in the direction of the applied field. The majority of the crystallites in the poled samples, however, still have their *b* axes preferentially oriented along the 2 direction. This shows that these samples are not poled to their maximum achievable polarization.

ACKNOWLEDGEMENT

JAD acknowledges support from Thorn-EMI during the period of this work. We also thank Professor I.M. Ward for help and encouragement.

REFERENCES

1 Ohigashi, H. and Koga, J. *Japan. J. Appl. Phys.* 1982, **21**, L455
2 Koga, K. and Ohigashi, H. *J. Appl. Phys.* 1986, **59**, 2142
3 Hasegawa, R., Takahashi, Y., Chatani, Y. and Tadokoro, H. *Polym. J.* 1982, **3**(5), 600
4 Tashiro, K., Takano, K., Kobayashi, M., Chatani, Y. and Tadokoro, H. *Polymer* 1984, **25**, 195

5 Tashiro, K., Takano, K., Kobayashi, M., Chatani, Y. and Tadokoro, H. *Ferroelectrics* 1984, **57**, 297
6 Naegele, D., Yoon, D. Y. and Broadhurst, M. G. *Macromolecules* 1978, **11**, 1279
7 Davis, G. T., McKinney, J. E., Broadhurst, M. G. and Roth, S. C. *J. Appl. Phys.* 1978, **49**, 4998
8 Kepler, R. G. and Anderson, R. A. *J. Appl. Phys.* 1978, **49**, 1232
9 Bur, A. J., Barnes, J. D. and Wahlstrand, K. J. *J. Appl. Phys.* 1986, **59**(7), 2345
10 Furukawa, T., Date, M., Fukada, E., Tajitsu, Y. and Chiba, A. *Japan. J. Appl. Phys.* 1980, **19**(2), L109
11 Yamada, T. and Kitayama, T. *J. Appl. Phys.* 1981, **52**(11), 6859
12 Yagi, T., Higashihata, Y., Furukawa, K. and Sako, J. *Ferroelectrics* 1984, **57**, 327
13 Furukawa, T., Date, M., Ohuchi, M. and Chiba, A. *J. Appl. Phys.* 1984, **56**(5), 1481
14 Tajitsu, Y., Ogura, H., Chiba, A. and Furukawa, T. *Japan. J. Appl. Phys.* 1987, **26**(4), 554
15 Luongo, J. P. *J. Polym. Sci. A-2* 1972, **10**, 1119
16 Naegele, D. and Yoon, D. Y. *Appl. Phys. Lett.* 1978, **33**, 132
17 Fukada, E., Date, M. and Furukawa, T. *Am. Chem. Soc. Org. Coat. Plast. Chem. Prepr.* 1978, **38**, 262
18 Broadhurst, M. G. and Davis, G. T. *Annu. Rep. Conf. Electr. Insul. Diel. Phen.* 1979, **48**, 447
19 Furukawa, T., Johnson, G. E., Blair, H. E., Tajitsu, Y., Chiba, A. and Fukada, E. *Ferroelectrics* 1981, **32**, 61
20 Servet, B., Ries, S., Broussoux, D. and Micheron, F. *J. Appl. Phys.* 1984, **55**(7), 2763
21 Takahashi, Y. and Odajima, A. *Ferroelectrics* 1981, **32**, 49; *Ferroelectrics* 1984, **57**, 221
22 Nakamura, K., Teramoto, Y. and Muruyama, N. *Ferroelectrics* 1984, **57**, 139
23 Douglas, D. C., McBrierty, V. J. and Wang, T. T. *J. Chem. Phys.* 1982, **77**(11), 5826
24 Buerger, M. J. 'X-ray Crystallography', Wiley, New York, 1962, p. 181